

## PAPER

# Facile, substrate-scale growth of mono- and few-layer homogeneous MoS<sub>2</sub> films on Mo foils with enhanced catalytic activity as counter electrodes in DSSCs

To cite this article: Aspasia Antonelou *et al* 2016 *Nanotechnology* **27** 045404

View the [article online](#) for updates and enhancements.

## You may also like

- [Chaotic behavior of new experimental data of the LTGP \(2004-2006\) confirm possible relation to seismic activity in Western Greece](#)  
K Giannakopoulos and A Ifantis
- [The synthesis mechanism of Mo<sub>3</sub>C on Ag-Cu alloy substrates by chemical vapor deposition and the impact of substrate choice](#)  
Katherine T Young, Colter Smith, Dale A Hitchcock *et al.*
- [Exploiting unsupervised and supervised classification for segmentation of the pathological lung in CT](#)  
P Korfiatis, C Kalogeropoulou, D Daoussis *et al.*



**ECS** The Electrochemical Society  
Advancing solid state & electrochemical science & technology

**247th ECS Meeting**  
Montréal, Canada  
May 18-22, 2025  
*Palais des Congrès de Montréal*

**Showcase your science!**

**Abstract submission deadline extended: December 20**

**ECS UNITED**

# Facile, substrate-scale growth of mono- and few-layer homogeneous MoS<sub>2</sub> films on Mo foils with enhanced catalytic activity as counter electrodes in DSSCs

Aspasia Antonelou<sup>1,2</sup>, George Syrokostas<sup>1</sup>, Lamprini Sygellou<sup>1</sup>,  
George Leftheriotis<sup>3</sup>, Vassileios Dracopoulos<sup>1</sup> and  
Spyros N Yannopoulos<sup>1</sup>

<sup>1</sup> Foundation for Research and Technology Hellas—Institute of Chemical Engineering Sciences (FORTH/ICE-HT), PO Box 1414, GR-26504, Rio-Patras, Greece

<sup>2</sup> Department of Materials Science, University of Patras, GR-26504, Rio-Patras, Greece

<sup>3</sup> Department of Physics, University of Patras, GR-26504, Rio-Patras, Greece

E-mail: [gesirokos@iceht.forth.gr](mailto:gesirokos@iceht.forth.gr) and [sny@iceht.forth.gr](mailto:sny@iceht.forth.gr)

Received 19 October 2015, revised 12 November 2015

Accepted for publication 20 November 2015

Published 14 December 2015



CrossMark

## Abstract

The growth of MoS<sub>2</sub> films by sulfurization of Mo foils at atmospheric pressure is reported. The growth procedure provides, in a controlled way, mono- and few-layer thick MoS<sub>2</sub> films with substrate-scale uniformity across square-centimeter area on commercial foils without any pre- or post-treatment. The prepared few-layer MoS<sub>2</sub> films are investigated as counter electrodes for dye-sensitized solar cells (DSSCs) by assessing their ability to catalyse the reduction of I<sub>3</sub><sup>-</sup> to I<sup>-</sup> in triiodide redox shuttles. The dependence of the MoS<sub>2</sub> catalytic activity on the number of monolayers is explored down to the bilayer thickness, showing performance similar to that of, and stability against corrosion better than, Pt-based nanostructured film. The DSSC with the MoS<sub>2</sub>–Mo counter electrode yields a photovoltaic energy conversion efficiency of 8.4%, very close to that of the Pt–FTO-based DSSC, i.e. 8.7%. The current results disclose a facile, cost-effective and green method for the fabrication of mechanically robust and chemically stable, few-layer MoS<sub>2</sub> on flexible Mo substrates and further demonstrate that efficient counter electrodes for DSSCs can be prepared at thicknesses down to the 1–2 nm scale.

Keywords: 2D crystals, transition metal dichalcogenides, cyclic voltammetry, Raman scattering, counter electrodes, dye-sensitized solar cells

(Some figures may appear in colour only in the online journal)

## 1. Introduction

Transition metal dichalcogenides (TMDCs) are a particular class of two-dimensional (2D) layered crystals [1, 2] which have attracted a tremendous amount of research interest over the last decade as rivals and successors of graphene [3]. Their layered structure is the result of primarily covalent bonding within the layer and weak van der Waals interlayer forces. The interest is not only academic as 2D TMDCs exhibit a number of unique phenomena exploitable in various applications.

TMDCs belong to the group of polyhedral thick 2D materials, where the plane of metal atoms is sandwiched between two layers of the chalcogen or halide atoms, as opposed to the single-atom thick (graphene BN) 2D crystals [4]. On general grounds, layered crystals can be considered as molecular crystals in which the 2D layer plays the role of the molecular unit. An early classification of the *molecularity* or the degree of the 2D character of TMDC materials was postulated by Zallen and Slade [5] more than 40 years ago, based on the magnitudes of interlayer–intralayer force-constant ratios.

MoS<sub>2</sub> is perhaps the first TMDC which has been the subject of systematic studies for several decades, since the work of Frindt and collaborators [6–9], as well as other groups [10] with respect to the isolation of single layers by mechanical and chemical exfoliation. To date, MoS<sub>2</sub> has been grown employing different synthesis routes such as liquid exfoliation [11, 12], chemical vapor deposition on a variety of substrates, primarily through the sulfurization of MoO<sub>3</sub> [13], decomposition of precursor compounds [14], and other methods [1, 2]. Sulfurization of Mo thin films predeposited on various substrates has also been followed as an alternative route to grow few-layer thick MoS<sub>2</sub> [15–17]. Recently, a detailed investigation of the influence of the substrate type, the film thickness and the reaction temperature was reported for the sulfurization of Mo thin films (up to 4 nm) [18]. Liquid exfoliation produces large volumes of MoS<sub>2</sub> nanoplatelets with lateral dimensions of few tens of nanometers. However, controlling the thickness size distribution is still a matter of investigation, while aggregation of nanoplatelets upon drop casting on a substrate is always an issue. Preparation methods based on thermal evaporation have demonstrated growth of MoS<sub>2</sub> layers either in fragmented structures (micrometer-sized crystals) or growth at wafer-scale dimensions [19]. They frequently require multistep preparation processes, long growth times, and expensive or specially prepared substrates, while controlling the uniformity of film thickness (number of monolayers) still remains a thorny issue even in the case of sulfurizing predeposited ultrathin Mo films [18].

Whilst a plethora of investigations regarding 2D MoS<sub>2</sub> has been directed towards its optical and electronic properties, much less attention has been paid to the catalytic activity of MoS<sub>2</sub> crystals and even less to monolayer and few-layer MoS<sub>2</sub>. Currently, there is a demand to replace the Pt-based counter electrodes (CEs) in dye-sensitized solar cells (DSSCs) due to certain disadvantages they present, such as high cost, especially in the case where a conductive glass substrate (FTO) is also used, partial detachment from the substrate, adsorption of iodide species leading to catalytic deactivation [20], and moderate performance when redox couples other than iodide–triiodide are used. In this context, TMDCs show great potential, as they offer a low-cost, reliable alternative solution considering the above shortcomings of Pt-based electrodes. However, current conditions to be fulfilled by Pt-free and FTO-free electrode materials include high catalytic activity and electrical conductivity, high specific area, corrosion/chemical stability, and ease in fabrication [21]. The potential of a variety of other materials such as carbon-based, transition metal compounds, conductive polymers, and hybrid nanomaterials performing as CEs has been reviewed recently [21]. The catalytic activity of hydrothermally grown MoS<sub>2</sub> and WS<sub>2</sub> crystals and their role as CEs in DSSCs have been explored only very recently. These sulfides have shown enhanced catalytic performance for the reduction of I<sub>3</sub><sup>-</sup> to I<sup>-</sup>; however, the crystal growth is lengthy (a few days) and the preparation procedure of the 20 μm thick MoS<sub>2</sub> films is quite laborious, involving several steps [22]. A few more studies have appeared over the last two years reporting efficiencies in the range 2–8.7% with the use of MoS<sub>2</sub> as the CE [23–28],

reaching in the best case [22] the efficiency of a DSSC with a platinized CE. In fact, the ratio of the efficiency of a device with a MoS<sub>2</sub> CE to that of a device with a Pt CE ranges from 0.3 to about 1. Besides, efforts have also been focused on combinations of MoS<sub>2</sub> with carbon-based nanomaterials (graphene, carbon nanotubes, etc), where in certain cases the above-mentioned ratio exceeds unity [29–35].

In general, high-efficiency DSSCs require films of the CE material much thicker than that of the Pt electrode [36]. In order to achieve efficiencies comparable with that of a Pt-based CE, the thickness of the MoS<sub>2</sub> film ranges from 100 nm to several micrometers. Notably, the influence of the number of MoS<sub>2</sub> monolayers on the catalytic activity of the CE has not been reported until now. Here, we show that preparation of substrate-wide MoS<sub>2</sub> layers is achievable with easy control down to the monolayer thickness. The growth takes place via controlled sulfurization of commercially available Mo foils across square-centimeter area, without any pre- or post-treatment, by a process that is scalable to any substrate dimension on the time scale of a few minutes. The quality of the prepared MoS<sub>2</sub> layers on flexible substrates is characterized by field-emission scanning electron microscopy (FE-SEM), Raman scattering, and x-ray photoelectron spectroscopy (XPS). Besides, the catalytic activity of MoS<sub>2</sub> has been evaluated by cyclic voltammetry (CV), demonstrating outstanding performance similar to, and stability better than, those of the more costly Pt-based film, even for two-layered films. DSSCs based on the MoS<sub>2</sub>–Mo counter electrode (CE) exhibit outstanding performance, similar to that of the Pt–FTO CE. This is the first time that a device with a few-layered MoS<sub>2</sub> counter electrode has exhibited efficiency comparable with that of a Pt–FTO CE.

## 2. Experiment

### 2.1. Sulfurization of Mo foils

Molybdenum foils were purchased from Alfa Aesar (99.95% purity, 0.05 mm thickness) and were used without any treatment. A three-zone horizontal tube furnace was used for the growth of MoS<sub>2</sub> on the surface of Mo foils. Specimens of 1.0 × 1.5 cm<sup>2</sup> were maintained at 800 °C, while an alumina boat loaded with high purity elemental sulfur was placed upstream several centimeters away from the substrates. The temperature and hence the vapor pressure of sulfur was used as the main factor controlling the number of MoS<sub>2</sub> monolayers. High purity Ar gas was used to purge the reaction tube for 1 h at a flow of 120 sccm before raising the temperature; the same gas flow was maintained during the growth process. The furnace was heated from ambient to 800 °C in about 20 min; it was kept at this temperature for a few minutes depending on the desired MoS<sub>2</sub> film thickness and then was turned off and left to cool down slowly before ceasing the gas purging. The presence of traces of oxygen gas was allowed in certain experiments in order to explore the role of the molybdenum oxide sublayer grown between the MoS<sub>2</sub> and the Mo substrate on the catalytic activity of the former.

Samples with increasing thickness are denoted as S-1, S-2, S-3, S-4, and S-5, which according to Raman and XPS data correspond to 1, 2, 3, and 4 ML and the bulk, respectively. Samples S-1, S-3, and S-5 contain an ultrathin oxide layer between the MoS<sub>2</sub> and the Mo substrate. S-1 and S-3 are prepared under the presence of traces of oxygen gas and have the structure MoS<sub>2</sub>-MoO<sub>2</sub>/MoO<sub>3</sub>-Mo, while S-2 and S-4 are prepared in the absence of oxygen and thus contain much less oxide sublayer.

## 2.2. Preparation of the Pt and TiO<sub>2</sub> films and DSSCs devices

Platinum films were prepared by electrodeposition from an aqueous H<sub>2</sub>PtCl<sub>6</sub> solution (0.002 M). A potentiostat-galvanostat (Autolab PGSTAT 204) and a three-electrode configuration were used with a SnO<sub>2</sub>:F glass (FTO) serving as the working electrode, an Ag-AgCl electrode as the reference and a Pt wire as the counter electrode. The electrodeposition process was carried out at a constant current of 0.5 mA cm<sup>-2</sup> for 200 s. As shown in our previous works [20, 37] the Pt films consist of distinct Pt nanoparticles with high surface area, ensuring an efficient catalytic action. TiO<sub>2</sub> films were prepared by the doctor-blade technique using TiO<sub>2</sub> nanoparticles (Degussa P25); details can be found elsewhere [38]. The thickness of the TiO<sub>2</sub> films, as measured by a profilometer (Ambios XP-1), was about 8 μm. TiO<sub>2</sub> films were soaked in an ethanol solution (0.3 mM) of the N719 dye (Dyesol) for 24 h. The DSSC devices were prepared according to our previous work [38], with the difference that the holes for inserting the liquid electrolyte (EL-HPE high performance electrolyte, Dyesol), were drilled from the side of the TiO<sub>2</sub>-FTO electrode. The effective DSSC area was 0.28–0.30 cm<sup>2</sup>.

## 2.3. Characterization of materials and devices

Electron microscopy images are recorded with the aid of a high resolution FE-SEM instrument (Zeiss, SUPRA 35VP) operating at 15 kV. Raman spectra are accumulated with the 441.6 nm laser line as the excitation source emerging from a He-Cd laser (Kimon). The scattered light is analyzed by a LabRam HR800 (Jobin Yvon) micro-Raman spectrometer at a spectral resolution of about 2.0 cm<sup>-1</sup>. A microscope objective with 50× magnification is used to focus the light onto a spot of about 3 μm in diameter. Low laser intensities were used (~0.37 mW on the sample) to avoid spectral changes due to heat-induced effects. The Raman shift was calibrated using the 520 cm<sup>-1</sup> Raman band of crystalline Si.

The surface analysis studies are performed in a UHV chamber ( $P < 10^{-9}$  mbar) equipped with a SPECS LHS-10 hemispherical electron analyzer. The XPS measurements are carried out using unmonochromatized Al K<sub>α</sub> radiation under conditions optimized for maximum signal (constant  $\Delta E$  mode with pass energy of 36 eV, giving a full width at half maximum (FWHM) of 0.9 eV for the Au 4f<sub>7/2</sub> peak). The analyzed area is an ellipsoid with dimensions 2.5 × 4.5 mm<sup>2</sup>. The XPS core level spectra are analyzed using a fitting

routine, which allows the decomposition of each spectrum into individual mixed Gaussian-Lorentzian components after a Shirley background subtraction. Errors in our quantitative data are found in the range of about 10% (peak areas) while the accuracy for BE assignments is about 0.1 eV.

Cyclic voltammetry was used in order to evaluate the electrocatalytic activity of the Pt-FTO and MoS<sub>2</sub>-Mo electrodes for the triiodide reduction. The composition of the electrolyte used for the cyclic voltammetry experiments was 10 mM KI, 1 mM I<sub>2</sub>, and 0.1 M LiClO<sub>4</sub> in propylene carbonate. The same three-electrode setup was used as for the electrodeposition and the sweep rate was 10 mV s<sup>-1</sup>. In order to evaluate the stability of the electrodes, up to 100 successive cycles were performed for a thin (>6–7 ML) and an ultrathin film (3 ML or equivalently 1.5–1.8 nm in thickness). Current-voltage (CV) curves were recorded during the cycles. The same electrolyte was used; however, the scan rate for the stability tests was set at 20 mV s<sup>-1</sup>.  $J$ - $V$  curves were recorded with the use of an Oriel 96000 solar simulator fitted with an AM1.5G filter, in conjunction with a Keithley 236 source meter. The incidence irradiance was 1000 W m<sup>-2</sup> as was measured by a Si photodiode (VTB8440B) calibrated with a Melles Griot 13PE001 broad band power meter [38].

## 3. Results and discussion

### 3.1. Characterization of film morphology and thickness uniformity

MoS<sub>2</sub> films grown with systematically increasing thickness are denoted as S-1, S-2, S-3, S-4, and S-5 (bulk); see the experimental section for details. Representative FE-SEM images revealing the morphology of MoS<sub>2</sub> films grown at different conditions are shown in figure 1. Image 1(a) shows the bare Mo substrate prior to the sulfurization reaction, illustrating the grainy texture of the surface. The mean grain size is between 200 and 300 nm. The morphology of the thin MoS<sub>2</sub> film (S-1), image 2(b), does not practically differ from the bare substrate texture. No appreciable morphological changes are observed either for the moderately sulfurized Mo foil (S-3), as depicted in image 1(c). In contrast, changes of the surface morphology are observed for the Mo foil sulfurized for longer periods (S-5); see image 2(d). In this case, growth of vertical (normal to the foil plane) structures are developed, which are reminiscent of such structures grown by CVD sulfurization of MoO<sub>3</sub>. The inset of image 2(d) illustrates another example of a Mo surface sulfurized for long times, where a high density of coin-like shaped crystals grown normal to the surface is evident.

Off-resonant Raman spectroscopy is a valuable, fast and reliable method for the evaluation of the number of MoS<sub>2</sub> monolayers based on the thickness dependence of the energy separation of two dominant Raman bands, as has been demonstrated first by Lee *et al* [39] and later by other groups [40], for mechanically exfoliated thin films. Far from resonance (1.96 eV for the bulk) four first-order Raman active

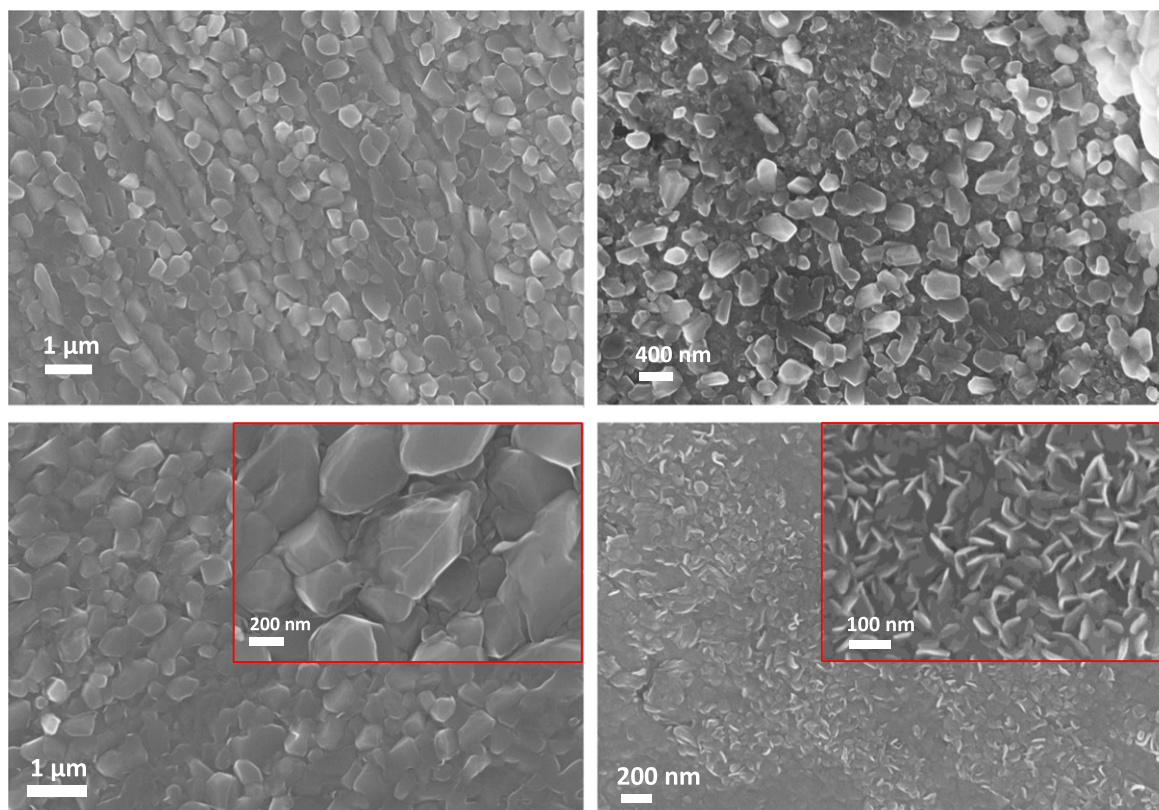


**Figure 1.** FE-SEM images of MoS<sub>2</sub> layers on Mo foils. (a) Bare Mo substrate. (b)–(d) MoS<sub>2</sub> layers with progressively increasing thickness, 1, 3, and more than 10 ML, respectively.

modes are observed at  $32\text{ cm}^{-1}$  ( $E_{2g}^2$ ),  $286\text{ cm}^{-1}$  ( $E_{2g}$ ),  $383\text{ cm}^{-1}$  ( $E_{2g}^1$ ), and  $408\text{ cm}^{-1}$  ( $A_{1g}$ ) [41]. The last two are the bands of interest, as their energy separation  $\Delta\omega = \omega(A_{1g}) - \omega(E_{2g}^1)$  is the main indicator used to infer the number of monolayers ( $nL$ ). Typical values of  $\Delta\omega$  for 1L, 2L, 3L, 4L, and bulk are  $18.5\text{--}19.5$ ,  $21.5\text{--}22.0$ ,  $23.1\text{--}23.3$ ,  $24.1\text{--}24.5$ , and  $25.5\text{ cm}^{-1}$ , respectively [39, 40]. Figure 2 illustrates the results of the Raman measurements and spectrum analyses. Figure 2(a) shows representative Raman spectra of the MoS<sub>2</sub> layers prepared by varying the degree of the Mo foil sulfurization. The values of the energy difference  $\Delta\omega$  shown in the legend demonstrate the effective control of the current atmospheric pressure CVD growth method on the number of MoS<sub>2</sub> MLs grown on the rough surface of the Mo foil. Since the correlation between  $\Delta\omega$  and the number of MLs was devised for free-standing, mechanically exfoliated layers, one might argue that differential peak shifts, due to stresses exerted on the MoS<sub>2</sub> layers by the Mo substrate, could render the correlation not useful for the present case. However, experimental and theoretical calculations [42] have shown that both the  $E_{2g}^1$  and  $A_{1g}$  Raman bands of strained monolayer and few-layer MoS<sub>2</sub> experience small redshifts. Besides, as the  $E_{2g}^1$  band shifts with a higher rate than the  $A_{1g}$  mode, strained layers show slightly larger  $\Delta\omega$  values and the estimated number of layers can be effectively slightly higher in strained films. Concluding, the  $\Delta\omega$  values reported above

for the present case are upper bounds of the  $\Delta\omega = \omega(A_{1g}) - \omega(E_{2g}^1)$  in the case of strain interference; the real  $\Delta\omega$  values would be expected to be even smaller.

A remarkable outcome of the grown MoS<sub>2</sub> layers is their thickness uniformity across the whole substrate area ( $1.5\text{--}2.0\text{ cm}^2$ ). Figures 2(b) and (c) show representative linear Raman mappings for the 1 ML (S-1) and the 3 ML (S-3) thick films, respectively, indicating the outstanding thickness uniformity of the prepared MoS<sub>2</sub> layers. Spectra were recorded along a line scan in  $5\text{ }\mu\text{m}$  steps. The corresponding  $\Delta\omega$  values for S-1 and S-3 are shown in figure 2(d). The same uniform behavior was observed for all films. Spectra were also recorded from various areas on the foils' surfaces across centimeter scale distances, exhibiting the same uniformity effect. The film thickness consistency, as inferred from the Raman spectra, is the same for both sides of the foils, which points to homogeneous coverage of the Mo foils with MoS<sub>2</sub> layers. Despite the rough foil surface the MoS<sub>2</sub> films show high crystallinity, as can be deduced from the narrow Raman line width, which amounts to about  $4\text{ cm}^{-1}$  for both the  $A_{1g}$  and the  $E_{2g}^1$  bands. Plausibly, the value for the  $E_{2g}^1$  mode is rather higher than that of the exfoliated free-standing layers due to the roughness of the Mo substrate. The presence of grain boundaries affects (reduces) crystal domains, which is the source of band broadening. On the other side, this surface roughness might be beneficial for the electrocatalytic activity

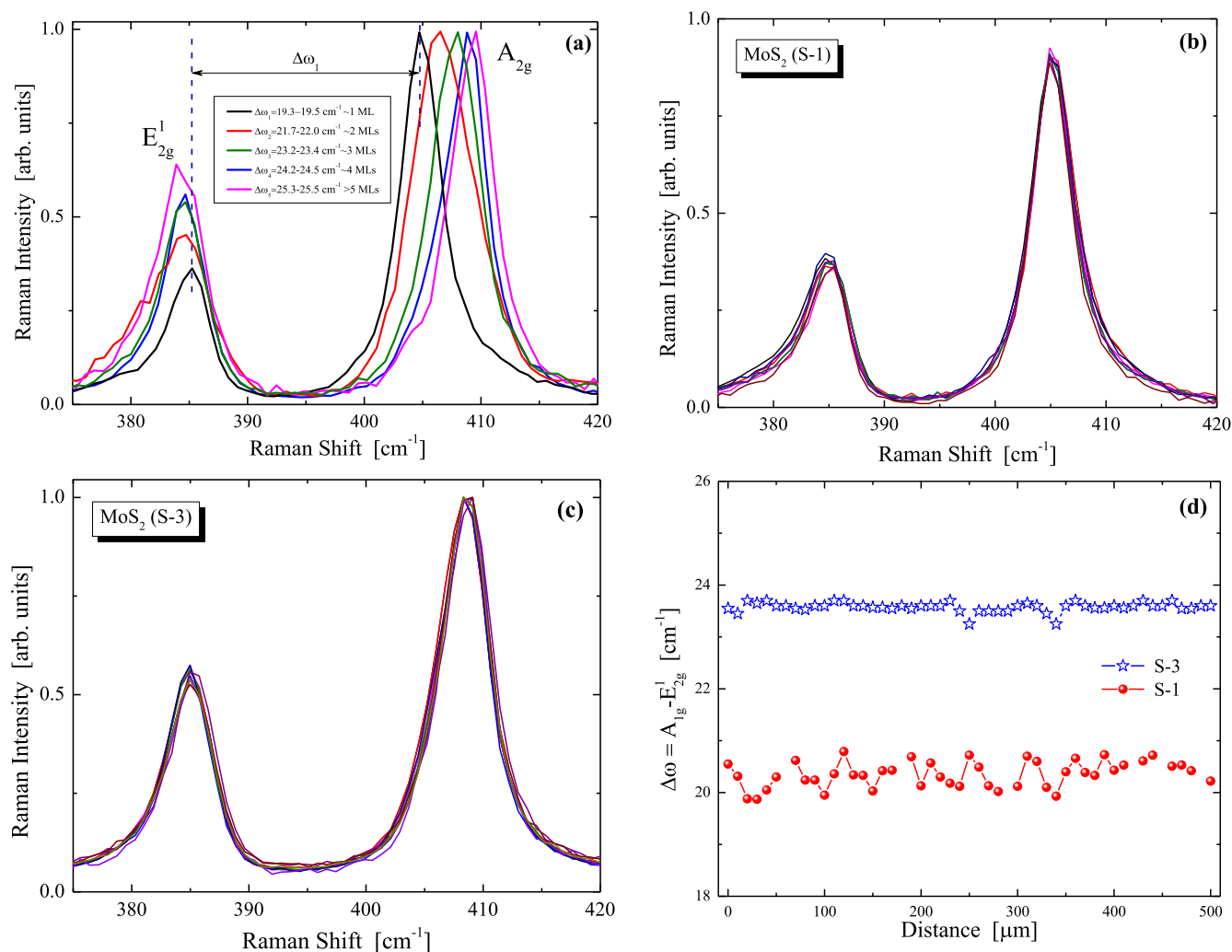


**Figure 2.** (a) Raman spectra of MoS<sub>2</sub> films grown on Mo foils with varying number of monolayers. (b) Series of Raman spectra along a line scan on S-1 (1 ML). (c) Series of Raman spectra along a line scan on S-3 (~3 ML). (d) Energy difference of the two Raman bands for the spectra that correspond to (b) and (c).

of the MoS<sub>2</sub> on Mo foil as the edge sites are the catalytically active ones, as discussed below.

The surface chemistry was investigated by XPS, which also provided a rough estimate of the number of MoS<sub>2</sub> monolayers for the various samples. From the survey scans of all specimens Mo, S, O, and C peaks are found. Figure 3 displays detailed XPS scans for the Mo 3d and the S 2p orbitals for the samples with different number of MoS<sub>2</sub> monolayers. The left column of figures 3(a)–(c) shows the Mo 3d peaks of the samples which were prepared in the presence of oxygen gas traces. For the thicker MoS<sub>2</sub> film (S-5), figure 3(a), a doublet at binding energy Mo 3d<sub>5/2</sub> 229.3 eV with a spin–orbit splitting of 3.2 eV is detected, which is attributed to Mo<sup>4+</sup>. Further, an S 2p<sub>3/2</sub> peak (figure 3(f)) at a binding energy of 161.9 ± 0.1 eV is observed, assigned to S in stoichiometric MoS<sub>2</sub> [43]. Moreover, the S:Mo element ratio estimated from the peak area of Mo 3d and S 2p spectra after correcting with the appropriate sensitivity factors is close to stoichiometric value, i.e. 2. The above results confirm the formation of MoS<sub>2</sub> with thickness more than about 12 nm since no signal

from the Mo substrate is detected. The results demonstrate the growth of stoichiometric 2H-MoS<sub>2</sub> and the absence of the 1T phase [11], as is also evidenced from the Raman spectra. The absence of peaks between 168 and 170 eV shows that no oxidized sulfur species are present.

Besides the aforementioned XPS peaks, samples S-1 and S-3 exhibit extra components at Mo 3d<sub>5/2</sub> binding energies of 232.6 and 231.1 eV, which are assigned to Mo in Mo<sup>6+</sup> (MoO<sub>3</sub>) and Mo<sup>4+</sup> (MoO<sub>2</sub>) chemical states, respectively [44]. The oxide layers are more evident in the case of the MoS<sub>2</sub> monolayer film (S-1). Although samples S-2 and S-4 were prepared under pure Ar purging, traces of MoO<sub>3</sub> oxide are present, as can be made out from figures 3(d) and (f). The lack of a MoO<sub>2</sub> layer and the reduced MoS<sub>2</sub> thickness of these samples make possible the detection of a new component at Mo 3d<sub>5/2</sub> binding energy 228.0 ± 0.1 eV assigned to Mo<sup>0</sup> [44].

The thicknesses of the sulfide and oxide layers have been estimated based on the intensities of the S 2p and Mo 3d peak components and using the appropriate sensitivity factors, equations, and parameters, as detailed elsewhere [45]. The

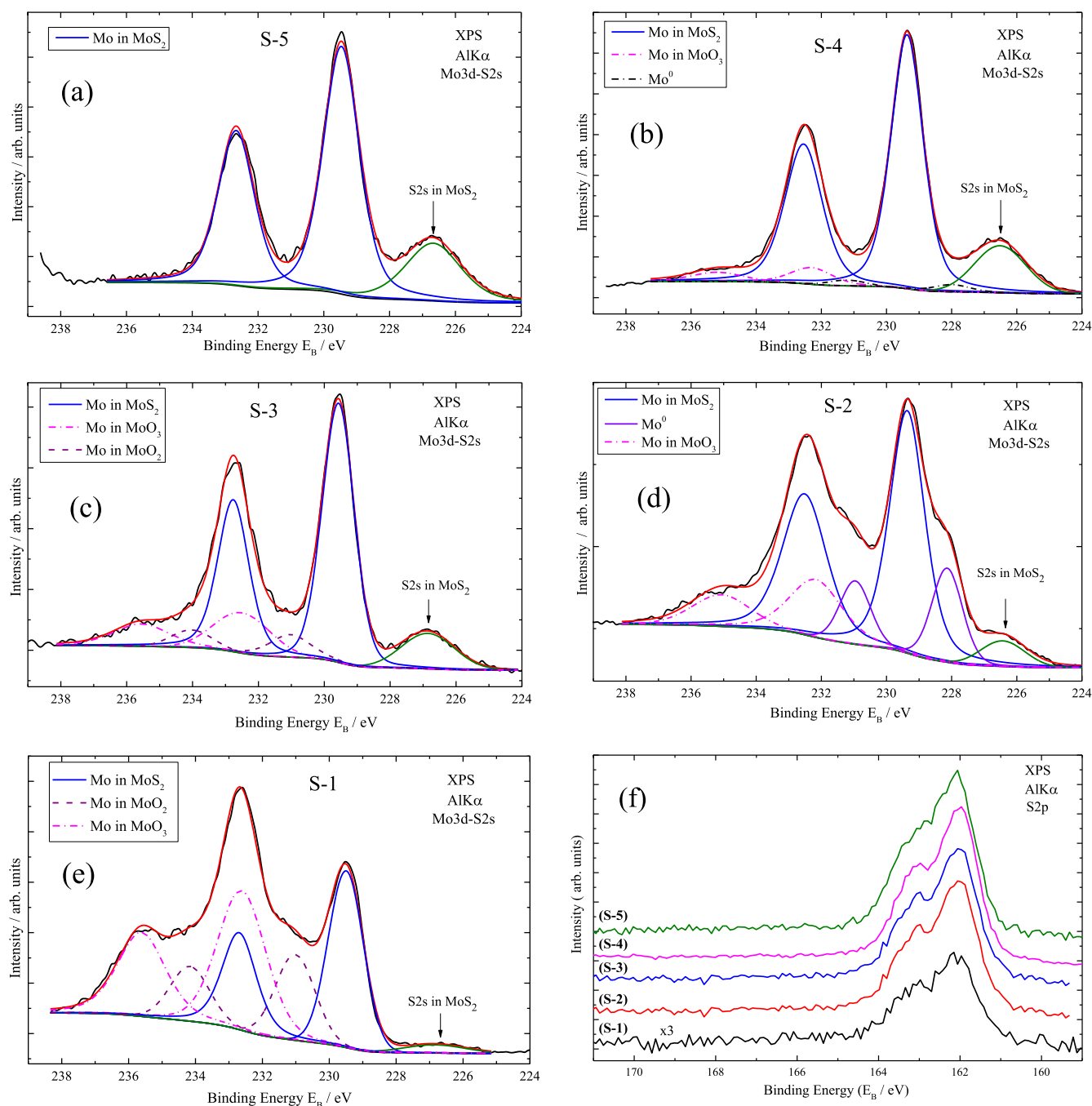


**Figure 3.** XPS spectra of core levels accumulated from the MoS<sub>2</sub> samples with various thicknesses. (a)–(e) Deconvoluted Mo 3d peaks and (f) S 2p peak.

**Table 1.** Number of MoS<sub>2</sub> monolayers as estimated from Raman scattering and thickness/number of monolayers as estimated by XPS analysis.

Sample	No of MLs (Raman)	MoS <sub>2</sub> thickness, nm ( $\pm 0.1$ nm)	No of MLs (XPS)
S-1	1	0.7	1
S-2	2	2.2	$\sim 3$
S-3	3	3.2	$\sim 4$
S-4	4	5.2	$\sim 7$
S-5	bulk	$> 12$	bulk

MoS<sub>2</sub> thicknesses of the various samples are compiled in table 1 together with the corresponding results obtained by Raman scattering. The thicknesses of the MoO<sub>2</sub> and MoO<sub>3</sub> sublayers, wherever present, are estimated to be about 3 nm and about 2 nm, respectively. While both the MoO<sub>2</sub> and the MoO<sub>3</sub> oxide are evident in the XPS spectra, only the former compound is measurable in the Raman spectra. This can be attributed to the laser excitation energy (441.6 nm or 2.8 eV), which is in resonance with the MoO<sub>2</sub>, whose optical bandgap is of about 2.65–2.80 eV [46].

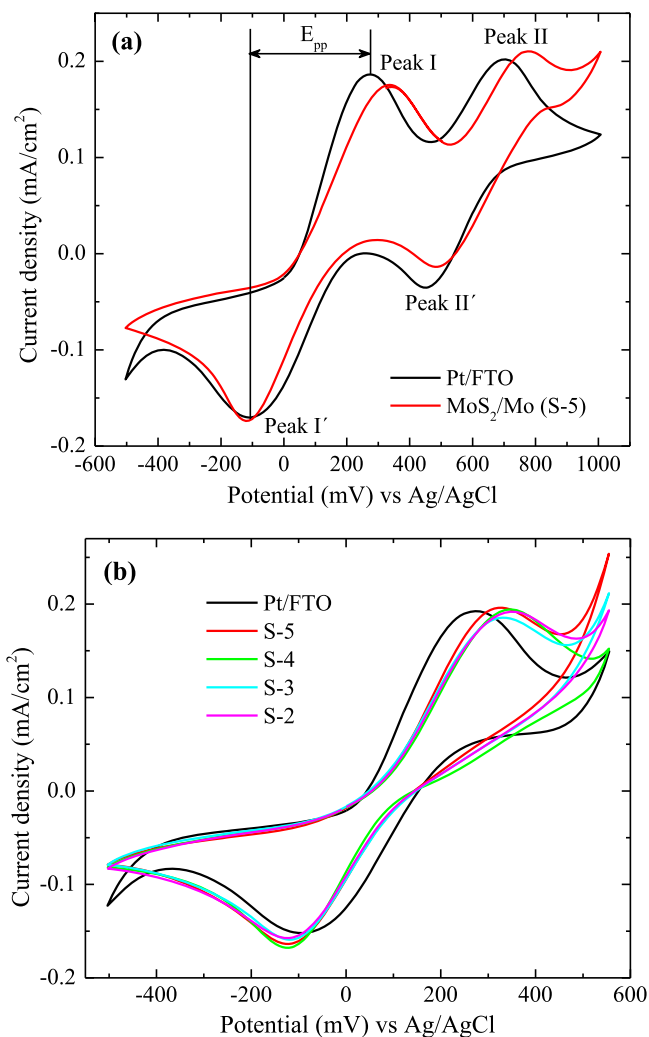
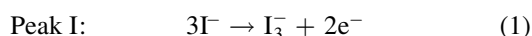


**Figure 4.** (a) Full range cyclic voltammogram for an electrodeposited Pt–FTO and a MoS<sub>2</sub>–Mo electrode. (b) Cyclic voltammograms for MoS<sub>2</sub>–Mo electrodes with different number of monolayers showing the left-hand pair of redox peaks.

### 3.2. Catalytic properties and photovoltaic performance

Cyclic voltammetry is employed to evaluate the catalytic activity of the various MoS<sub>2</sub> films [20]. In particular, we explore the role of the number of MLs and the presence of the oxide sublayer in the catalytic performance of the material. Characteristic CVs for an electrodeposited Pt–FTO electrode and for a MoS<sub>2</sub>–Mo electrode are shown in figure 4(a). The primary role of the CE is to catalyze the reduction of I<sub>3</sub><sup>-</sup> to I<sup>-</sup>; therefore we focus on the left-hand pair of peaks of the CV (I and I'). This pair corresponds to anodic (peak I, oxidation) and the cathodic (peak I', reduction) processes. The current density peaks correspond to the following chemical reactions.



The reduction of triiodide (reaction 2) is of particular importance here, since it takes place on the counter electrode of a DSSC during operation. The CV curves of the MoS<sub>2</sub>

films bear a close resemblance to that of Pt (peak positions and current densities), suggesting similar catalytic activity for the reduction of I<sub>3</sub><sup>-</sup>.

The peak current density,  $I_p$ , calculated for MoS<sub>2</sub> and Pt, is shown in table 2. We observe that the two electrodes exhibit nearly the same peak current density for the reduction of triiodide, indicating comparable electrochemical properties between the two electrodes. Based on the  $I_p$  values, the diffusion coefficient for triiodide is calculated using the Randles–Sevcik equation:

$$I_p = (2.69 \times 10^5) n^{3/2} A D_a^{1/2} C_0^* \nu^{1/2} \quad (3)$$

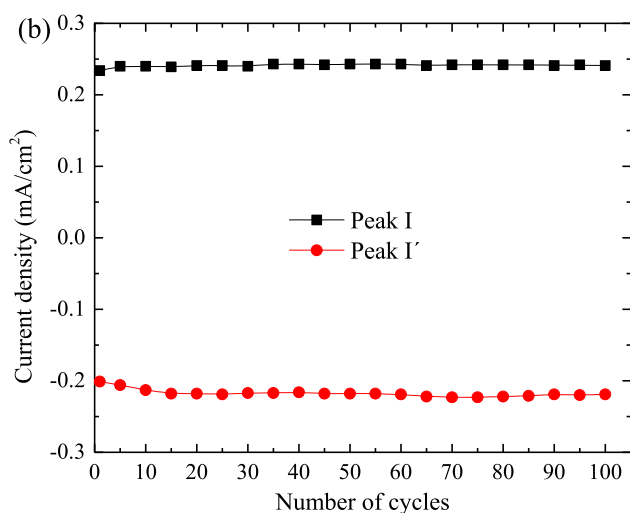
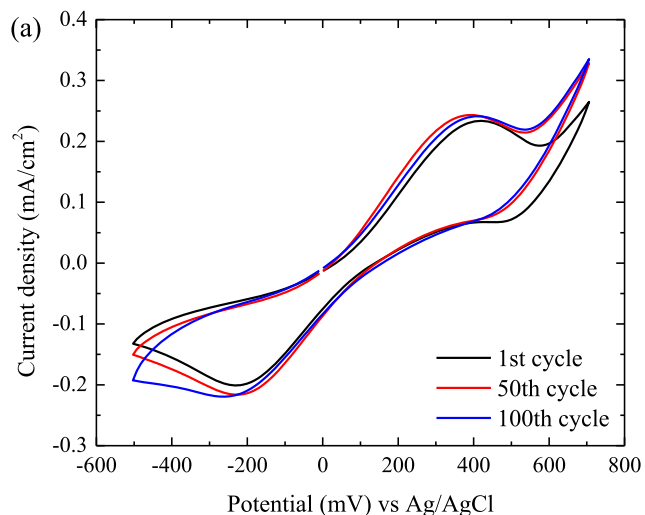
where  $n$  is the number of electrons involved in the reaction,  $A$  is the electrode surface,  $D_a$  stands for the diffusion coefficient,  $C_0^*$  represents the bulk concentration of the triiodide ions, and  $\nu$  is the scan rate. The diffusion coefficient for triiodide ions is comparable for the two cases. The somewhat lower value of the peak-to-peak potential ( $E_{pp}$ ) for Pt–FTO, in relation to the MoS<sub>2</sub>–Mo electrode, implies that the redox reactions have a slightly higher reaction rate in the former. Therefore, the catalytic activity of the MoS<sub>2</sub>–Mo electrode is comparable to that of a Pt–FTO electrode, with a minor difference in the reaction rate.

The cyclic voltammograms of various MoS<sub>2</sub>–Mo electrodes with variable thickness, from 2 ML to bulk, are shown in figure 4(b). It is evident that all electrodes exhibit nearly the same catalytic activity toward triiodide reduction. This suggests that the number of MoS<sub>2</sub> monolayers for such ultrathin films, prepared on Mo foil by atmospheric pressure CVD, does not appreciably influence the electrocatalytic properties of the material. This observation is in stark contrast with the conception that CE films with enhanced catalytic activity should be much thicker than the Pt electrode [36], and places emphasis on the role of the catalytically active edges. The current findings can account for the wide range of MoS<sub>2</sub> film thicknesses that have been prepared by others (ranging from a few tens of nanometers up to 20  $\mu\text{m}$ ) as CEs for DSSCs. Further, the presence of the oxides sublayers does not seem to affect the electrocatalytic properties, as long as two monolayers have been grown. In the case of 1 ML of MoS<sub>2</sub> the oxide presence seems significant.

Apart from the electrocatalytic activity, the stability issue of the CE is also an important factor. A thin MoS<sub>2</sub> layer (composed of more than 6–7 ML) and an ultrathin one with 3 ML—or equivalently 1.5–1.8 nm in thickness—were tested in two ways. (i) Long term corrosion tests in the electrolyte for at least 2 months. CVs were recorded at frequent periods, demonstrating the robustness of the MoS<sub>2</sub> layers. (ii) Stability of the electrochemical response of MoS<sub>2</sub> electrode for 100 successive cycles. Typical CV curves and the variation of the peak current density in the course of 100 successive cycles are shown in figures 5(a) and (b), respectively. As can be made out from these data, the CV curve shape remains almost unaffected while no significant variation is observed for both peak current densities, even after 100 polarization cycles. It is therefore confirmed that MoS<sub>2</sub> ultrathin film, with thickness less than 2 nm, exhibits excellent electrochemical stability,

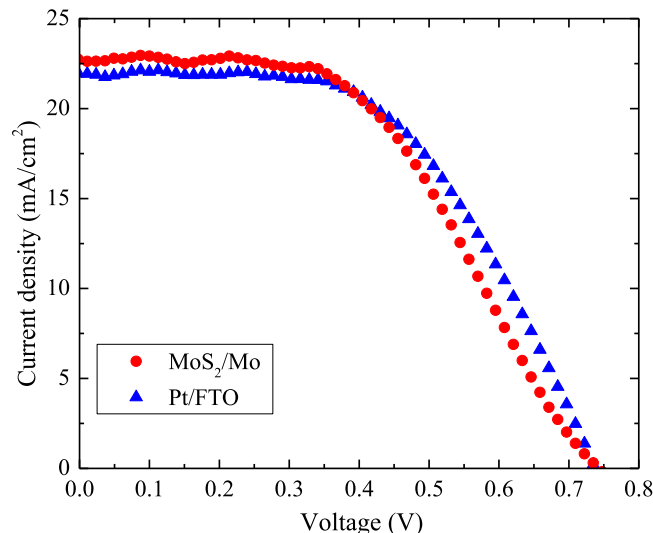
**Table 2.** Parameters related to catalytic activity of Pt-FTO and MoS<sub>2</sub>-Mo (S-5) extracted from the CV analysis.

Electrode	$I_p$ (mA cm <sup>-2</sup> )	$E_p$ (mV)	$E_{pp}$ (mV)	$D$ (10 <sup>-6</sup> cm <sup>2</sup> s <sup>-1</sup> )
Pt-FTO	-0.170	-110.1	383	4.99
MoS <sub>2</sub> -Mo	-0.174	-120.8	454	5.23

**Figure 5.** (a) Representative CV curves of the 3 ML thick MoS<sub>2</sub> film for the first, 50th, and 100th cycles. (b) Variation of the peak current density in the course of 100 successive cycles (scan rate: 20 mV s<sup>-1</sup>). Data points are presented with 5 cycle steps.

which is comparable to that of the nanostructured Pt electrode [47] and much thicker (100 nm) wet-chemically deposited MoS<sub>2</sub> films [24].

The photocurrent density–voltage ( $J$ – $V$ ) curves of the DSSCs using MoS<sub>2</sub>-Mo and Pt-FTO CEs are shown in figure 6. The corresponding photovoltaic properties are summarized in table 3. The measurements have been conducted using the experimental setup described in section 2.2 and in more detail in [38]. We observe an enhanced efficiency,  $\eta$ , of the cell with the MoS<sub>2</sub>-Mo CE, which is comparable to that using the Pt-FTO CE, with the difference in  $\eta$  being less than 3.5%. As the TiO<sub>2</sub> photoanode films of the

**Figure 6.** Comparison between the  $J$ – $V$  curves of DSSCs with a Pt-FTO (solid triangles) and a MoS<sub>2</sub>-Mo (solid circles) CE sensitized by N719 dye (0.3 mM in ethanol). (Intensity 1000 W/m<sup>2</sup>, Oriol 96000 solar simulator fitted with an AM 1.5G filter, area of the cells 0.28–0.3 cm<sup>2</sup>.)**Table 3.** Photovoltaic properties of DSSCs with a Pt-FTO and a MoS<sub>2</sub>-Mo CE.

CEs	$J_{sc}$ (mA cm <sup>-2</sup> )	$V_{oc}$ (V)	FF	$\eta$ %
Pt-FTO	21.9	0.735	0.534	8.7
MoS <sub>2</sub> -Mo	22.6	0.74	0.5	8.4

devices were prepared and sensitized to nearly identical conditions and the same electrolyte solution was used, any changes in the efficiency reflect mainly the performance of the CE. A small increment for the short circuit current density can be attributed to the better utilization of the solar light in the case of the non-transparent MoS<sub>2</sub>-Mo electrode causing reflection of incident photons back to the sensitized TiO<sub>2</sub> film [48]. On the other hand, the non-optimal geometry of the electrodes, regarding the distance between the nanostructured TiO<sub>2</sub> film and the ohmic contact (greater than 10 mm), is one of the factors responsible for the low values of the fill factor (FF) observed in both cases [49].

The fact that the MoS<sub>2</sub> CE is supported on the Mo metal foil provides a competitive advantage over the corresponding Pt-FTO construction as the Mo support engenders enhanced conductivity due to small ohmic series resistance in comparison to FTO. The few-monolayer MoS<sub>2</sub> films in the present case are not only responsible for the electrocatalytic activity, since for a bare Mo foil no current peaks appear in

cyclic voltammetry, but also offer an extra advantage as regards to the reduced charge transport resistance across the film thickness and the significant increase of the electrical conductivity as the film thickness reaches the few-nanometer scale. Indeed, it was recently shown for MoSe<sub>2</sub> that, with the film thickness decreasing from 2.7 μm to 6 nm, the electrical conductivity increases by more than two orders of magnitude [50]. Concluding, the prepared MoS<sub>2</sub>-Mo CEs bear electrochemical properties comparable to those of the Pt-based CE and an increased electrical conductivity, but on the other hand suffer from a reduced reaction rate. Besides, as CV reveals, the position of the peak current density is slightly more negative in the case of the MoS<sub>2</sub>-Mo CE, indicating a somewhat larger overpotential for the reduction of triiodide ions. These two factors might be responsible for the difference in the FF values.

The electrocatalytic properties of nanostructured MoS<sub>2</sub> have been under investigation for more than a decade. The catalytically active sites of single-layer MoS<sub>2</sub> nanoparticles used for hydrodesulfurization [51] and hydrogen evolution [52] have been identified by atomically resolved scanning tunneling microscopy and density functional theory studies. The role of the fully sulfided edges of single-layer MoS<sub>2</sub> nanoclusters was appreciated in those studies. In this direction, enhanced electrocatalytic properties of MoS<sub>2</sub> have been achieved by engineering the surface structure of MoS<sub>2</sub> to expose a higher number of edge sites by synthesizing a highly ordered double-gyroid MoS<sub>2</sub> bicontinuous network [53]. More recently, Lee *et al* [25] investigated the catalytic activity of MoSe<sub>2</sub> CEs in DSSCs preparing the chalcogenide material by a conceptually different approach than that adopted in the current work. They deposited 1 μm thick Mo film on glass and selenized its surface up to 70 nm deep, thus creating a MoSe<sub>2</sub> film of more than 100 ML, while the Mo unreacted sublayer plays the role of the transparent conductive oxide. The MoSe<sub>2</sub> film exhibits better catalytic activity than the Pt-based one (lower  $E_{pp}$  value and higher peak current density) and the corresponding DSSC device using MoSe<sub>2</sub>, as the CE showed PCE of 9.00% in comparison to 8.68% of the device using the Pt CE. The performance enhancement was attributed to the increase of the FF, which is associated with the better conductivity of the Mo sublayer in relation to the FTO in the Pt-based device. Thicker MoSe<sub>2</sub> films prepared at slightly higher temperature showed appreciably lower PCE, which was assigned [25] to the reduced number of edge sites of the layers which constitute the catalytically active area compared to the inert basal sites [51, 52].

An attempt to relate the DSSC efficiency with the morphology and the thickness of the MoS<sub>2</sub> CE was reported by Lei *et al* [26], who compared various MoS<sub>2</sub> electrodes composed of a few layers, multiple layers, and nanoparticles prepared by liquid exfoliation and spray coating on FTO. It was found that the electrocatalytic activity and the solar cell efficiency decreased progressively in the order nanoparticle → multi-layer → few-layer structures, which was attributed to the different numbers of catalytically active sites of the various electrode structures. In contrast, the current study shows no particular catalytic activity dependence on the

number of MoS<sub>2</sub> monolayers. We suggest that the existence of a grainy texture of the Mo foil surface is the key to the growth of MoS<sub>2</sub> nanocrystals with an enhanced number of edges acting as the catalytically active sites.

#### 4. Conclusions

A novel method for the fast, reliable, and controlled growth of few-monolayer thick MoS<sub>2</sub> layers by sulfurizing commercially available Mo flexible foils is presented. The method is cost effective and environmentally friendly as it employs atmospheric pressure CVD, is implemented in the time scale of a few minutes, and does not demand special pre- or post-treatment procedures. Excellent layer thickness uniformity of the various MoS<sub>2</sub> films is verified by Raman scattering mapping. It is further demonstrated that these MoS<sub>2</sub>-Mo constructions exhibit excellent catalytic properties in triiodide redox shuttles similar to those of the most costly Pt-based nanostructured films deposited on FTO substrates. In contrast to existing methods, where the MoS<sub>2</sub> layers are deposited on various substrates, thus suffering from mechanical stability problems, in the present case the reaction of S atoms with the Mo metal results in a mechanically robust structure with no detachment shortcomings. Notably, MoS<sub>2</sub> layers with thickness down to 1–2 nm exhibit long term chemical stability in the electrolyte solution comparable to that of the Pt nanostructured film. Cycling voltammograms show no appreciable dependence of the MoS<sub>2</sub> catalytic activity on the number of monolayers, even up to bilayer thickness. The nature of the grainy texture of the Mo foil surface is likely the key to the exceptional catalytic activity of the few-nanometer thick MoS<sub>2</sub> films, as it offers an increased number of catalytically active sites (layer edges). Despite the ultrathin nature of the MoS<sub>2</sub> films, the photovoltaic energy conversion of DSSCs fabricated with the MoS<sub>2</sub>-Mo CE yields an outstanding efficiency of 8.4%, which is very close to that of the Pt-FTO-based DSSC, i.e. 8.7%. The current findings open new avenues in the preparation of novel CE-TCO constructions, where the MoS<sub>2</sub>-Mo one can substitute the Pt-FTO combination given that the conductive glass substrate is the third more expensive material in a DSSC [54]. Optimization of DSSC energy conversion would benefit from the role of a more conductive substrate (Mo versus FTO) and an enhancement of light reflection from the MoS<sub>2</sub>-Mo surface in comparison to the nanostructured-Pt-FTO construction causing stronger light scattering.

#### Acknowledgments

GS, VD, and SNY acknowledge financial support from the PROENYL project (KRIPIS action) funded by Greece and the European Regional Development Fund of the European Union under the OP Competitiveness and Entrepreneurship.

## References

- [1] Xu M, Liang T, Shi M and Chen H 2013 Graphene-like two-dimensional materials *Chem. Rev.* **113** 3766–98
- [2] Butler S Z *et al* 2013 Progress, challenges, and opportunities in two-dimensional materials beyond graphene *ACS Nano* **7** 2898–926
- [3] Novoselov K S, Fal'ko V I, Colombo L, Gellert P R, Schwab M G and Kim K 2012 A roadmap for graphene *Nature* **490** 192–200
- [4] Nicolosi V, Chhowalla M, Kanatzidis M G, Strano M S and Coleman J N 2013 Liquid exfoliation of layered materials *Science* **340** 1226419
- [5] Zallen R and Slade M 1974 Rigid-layer modes in chalcogenide crystals *Phys. Rev. B* **9** 1627–37
- [6] Frindt R F 1966 Single crystals of MoS<sub>2</sub> several molecular layers thick *J. Appl. Phys.* **37** 1928
- [7] Joensen P, Frindt R F and Morrison S R 1986 Single-layer MoS<sub>2</sub> *Mater. Res. Bull.* **21** 457–61
- [8] Divigalpitaya W M R, Morrison S R and Frindt R F 1990 Thin oriented films of molybdenum disulphide *Thin Solid Films* **186** 177–92
- [9] Yang D, Sandoval S J, Divigalpitaya W M R, Irwin J C and Frindt R F 1991 Structure of single-molecular-layer MoS<sub>2</sub> *Phys. Rev. B* **43** 12053–6
- [10] Schumacher A, Scandella L, Kruse N and Prins R 1993 Single-layer MoS<sub>2</sub> on mica: studies by means of scanning force microscopy *Surf. Sci. Lett.* **289** L595–8
- [11] Eda G, Yamaguchi H, Voiry D, Fujita T, Chen M and Chhowalla M 2011 Photoluminescence from chemically exfoliated MoS<sub>2</sub> *Nano Lett.* **11** 5111–6
- [12] Coleman J N *et al* 2011 Two-dimensional nanosheets produced by liquid exfoliation of layered materials *Science* **331** 568–71
- [13] Lee Y-H *et al* 2012 Synthesis of large-area MoS<sub>2</sub> atomic layers with chemical vapor deposition *Adv. Mater.* **24** 2320–5
- [14] Liu K-K *et al* 2012 Growth of large-area and highly crystalline MoS<sub>2</sub> thin layers on insulating substrates *Nano Lett.* **12** 1538–44
- [15] Jäger-Waldau A, Lux-Steiner M C, Bucher E, Scandella L, Schumacher A and Prins R 1993 MoS<sub>2</sub> thin films prepared by sulphurization *Appl. Surf. Sci.* **65-66** 465–72
- [16] Lee K, Gatensby R, McEvoy N, Hallam T and Duesberg G S 2013 High-performance sensors based on molybdenum disulfide thin films *Adv. Mater.* **25** 6699–702
- [17] Zhan Y, Liu Z, Najmaei S, Ajayan P M and Lou J 2012 Large-area vapor-phase growth and characterization of MoS<sub>2</sub> atomic layers on a SiO<sub>2</sub> substrate *Small* **8** 966–71
- [18] Liu H, Ansah Antwi K K, Ying J, Chua S and Chi D 2014 Towards large area and continuous MoS<sub>2</sub> atomic layers via vapor-phase growth: thermal vapor sulfurization *Nanotechnology* **25** 405702
- [19] Kang K, Xie S, Huang L, Han Y, Huang P Y, Mak K F, Kim C-J, Muller D and Park J 2015 High-mobility three-atom-thick semiconducting films with wafer-scale homogeneity *Nature* **520** 656–60
- [20] Syrokostas G, Siokou A, Leftheriotis G and Yianoulis P 2012 Degradation mechanisms of Pt counter electrodes for dye sensitized solar cells *Sol. Energy Mater. Sol. Cells* **103** 119–27
- [21] Yun S, Hagfeldt A and Ma T 2014 Pt-free counter electrode for dye-sensitized solar cells with high efficiency *Adv. Mater.* **26** 6210–37
- [22] Wu M, Wang Y, Lin X, Yu N, Wang L, Wang L, Hagfeldt A and Ma T 2011 Economical and effective sulfide catalysts for dye-sensitized solar cells as counter electrodes *Phys. Chem. Chem. Phys.* **13** 19298
- [23] Al-Mamun M, Zhang H, Liu P, Wang Y, Cao J and Zhao H 2014 Directly hydrothermal growth of ultrathin MoS<sub>2</sub> nanostructured films as high performance counter electrodes for dye-sensitized solar cells *RSC Adv.* **4** 21277
- [24] Patil S A, Kalode P Y, Mane R S, Shinde D V, Doyoung A, Keumnam C, Sung M M, Ambade S B and Han S-H 2014 Highly efficient and stable DSSCs of wet-chemically synthesized MoS<sub>2</sub> counter electrode *Dalton Trans.* **43** 5256
- [25] Lee L T L, He J, Wang B, Ma Y, Wong K Y, Li Q, Xiao X and Chen T 2014 Few-layer MoSe<sub>2</sub> possessing high catalytic activity towards iodide/tri-iodide redox shuttles *Sci. Rep.* **4** 4063
- [26] Lei B, Li G R and Gao X P 2014 Morphology dependence of molybdenum disulfide transparent counter electrode in dye-sensitized solar cells *J. Mater. Chem. A* **2** 3919
- [27] Zhang J, Najmaei S, Lin H and Lou J 2014 MoS<sub>2</sub> atomic layers with artificial active edge sites as transparent counter electrodes for improved performance of dye-sensitized solar cells *Nanoscale* **6** 5279–83
- [28] Cheng C-K and Hsieh C-K 2015 Electrochemical deposition of molybdenum sulfide thin films on conductive plastic substrates as platinum-free flexible counter electrodes for dye-sensitized solar cells *Thin Solid Films* **584** 52–60
- [29] Liu C-J, Tai S-Y, Chou S-W, Yu Y-C, Chang K-D, Wang S, Chien F S-S, Lin J-Y and Lin T-W 2012 Facile synthesis of MoS<sub>2</sub>/graphene nanocomposite with high catalytic activity toward triiodide reduction in dye-sensitized solar cells *J. Mater. Chem.* **22** 21057
- [30] Yue G, Lin J-Y, Tai S-Y, Xiao Y and Wu J 2012 A catalytic composite film of MoS<sub>2</sub>/graphene flake as a counter electrode for Pt-free dye-sensitized solar cells *Electrochim. Acta* **85** 162–8
- [31] Tai S-Y, Liu C-J, Chou S-W, Chien F S-S, Lin J-Y and Lin T-W 2012 Few-layer MoS<sub>2</sub> nanosheets coated onto multi-walled carbon nanotubes as a low-cost and highly electrocatalytic counter electrode for dye-sensitized solar cells *J. Mater. Chem.* **22** 24753
- [32] Lin J-Y, Yue G, Tai S-Y, Xiao Y, Cheng H-M, Wang F-M and Wu J 2013 Hydrothermal synthesis of graphene flake embedded nanosheet-like molybdenum sulfide hybrids as counter electrode catalysts for dye-sensitized solar cells *Mater. Chem. Phys.* **143** 53–9
- [33] Yue G, Wu J, Xiao Y, Huang M, Lin J and Lin J-Y 2013 High performance platinum-free counter electrode of molybdenum sulfide-carbon used in dye-sensitized solar cells *J. Mater. Chem. A* **1** 1495–501
- [34] Yue G, Zhang W, Wu J and Jiang Q 2013 Glucose aided synthesis of molybdenum sulfide/carbon nanotubes composites as counter electrode for high performance dye-sensitized solar cells *Electrochim. Acta* **112** 655–62
- [35] Lin J-Y, Chan C-Y and Chou S-W 2013 Electrophoretic deposition of transparent MoS<sub>2</sub>-graphene nanosheet composite films as counter electrodes in dye-sensitized solar cells *Chem. Commun.* **49** 1440
- [36] Lee K S, Lee H K, Wang D H, Park N-G, Lee J Y, Park O O and Park J H 2010 Dye-sensitized solar cells with Pt- and TCO-free counter electrodes *Chem. Commun.* **46** 4505
- [37] Leftheriotis G, Syrokostas G and Yianoulis P 2012 'Partly covered' photoelectrochromic devices with enhanced coloration speed and efficiency *Sol. Energy Mater. Sol. Cells* **96** 86–92
- [38] Syrokostas G, Leftheriotis G and Yianoulis P 2014 Effect of acidic additives on the structure and performance of TiO<sub>2</sub> films prepared by a commercial nanopowder for dye-sensitized solar cells *Renew. Energy* **72** 164–73
- [39] Lee C, Yan H, Brus L E, Heinz T F, Hone J and Ryu S 2010 Anomalous lattice vibrations of single- and few-layer MoS<sub>2</sub> *ACS Nano* **4** 2695–700

- [40] Li H, Zhang Q, Yap C C R, Tay B K, Edwin T H T, Olivier A and Baillargeat D 2012 From bulk to monolayer MoS<sub>2</sub>: evolution of Raman scattering *Adv. Funct. Mater.* **22** 1385–90
- [41] Wieting T J and Verble J L 1971 Infrared and Raman studies of long-wavelength optical phonons in hexagonal MoS<sub>2</sub> *Phys. Rev. B* **3** 4286–92
- [42] Rice C, Young R J, Zan R, Bangert U, Wolverson D, Georgiou T, Jalil R and Novoselov K S 2013 Raman-scattering measurements and first-principles calculations of strain-induced phonon shifts in monolayer MoS<sub>2</sub> *Phys. Rev. B* **87** 081307
- [43] Galtayries A, Wisniewski S and Grimblot J 1997 Formation of thin oxide and sulphide films on polycrystalline molybdenum foils: characterization by XPS and surface potential variations *J. Electron Spectrosc. Relat. Phenomena* **87** 31–44
- [44] Brox B and Olefjord I 1988 ESCA studies of MoO<sub>2</sub> and MoO<sub>3</sub> *Surf. Interface Anal.* **13** 3–6
- [45] Sygellou L, Tielens H, Adelman C and Ladas S 2012 An x-ray photoelectron spectroscopy study of strontium-titanate-based high-k film stacks *Microelectron. Eng.* **90** 138–40
- [46] Patil R S, Uplane M D and Patil P S 2006 Structural and optical properties of electrodeposited molybdenum oxide thin films *Appl. Surf. Sci.* **252** 8050–6
- [47] Tang Z, Tang Q, Wu J, Li Y, Liu Q, Zheng M, Xiao Y, Yue G, Huang M and Lin J 2012 Template-free synthesis of a hierarchical flower-like platinum counter electrode and its application in dye-sensitized solar cells *RSC Adv.* **2** 5034
- [48] Zhang N N, Zhang B, Li Y H, Hou Y, Yang S, Zhong J H and Yang H G 2014 *In situ* growth of mirror-like platinum as highly-efficient counter electrode with light harvesting function for dye-sensitized solar cells *J. Mater. Chem. A* **2** 1641–6
- [49] Lee W J, Ramasamy E and Lee D Y 2009 Effect of electrode geometry on the photovoltaic performance of dye-sensitized solar cells *Sol. Energy Mater. Sol. Cells* **93** 1448–51
- [50] Chen R-S, Tang C-C, Shen W-C and Huang Y-S 2014 Thickness-dependent electrical conductivities and ohmic contacts in transition metal dichalcogenides multilayers *Nanotechnology* **25** 415706
- [51] Lauritsen J V, Nyberg M, Nørskov J K, Clausen B S, Topsøe H, Lægsgaard E and Besenbacher F 2004 Hydrodesulfurization reaction pathways on MoS<sub>2</sub> nanoclusters revealed by scanning tunneling microscopy *J. Catal.* **224** 94–106
- [52] Jaramillo T F, Jorgensen K P, Bonde J, Nielsen J H, Horch S and Chorkendorff I 2007 Identification of active edge sites for electrochemical H<sub>2</sub> evolution from MoS<sub>2</sub> nanocatalysts *Science* **317** 100–2
- [53] Kibsgaard J, Chen Z, Reinecke B N and Jaramillo T F 2012 Engineering the surface structure of MoS<sub>2</sub> to preferentially expose active edge sites for electrocatalysis *Nat. Mater.* **11** 963–9
- [54] Baxter J B 2012 Commercialization of dye sensitized solar cells: present status and future research needs to improve efficiency, stability, and manufacturing *J. Vac. Sci. Technol. A* **30** 020801